Thermodynamic Equilibrium of Domains in a Two-Component Langmuir Monolayer

Yufang Hu,*† Kieche Meleson,*† and Jacob Israelachvili†
*Department of Chemistry and Biochemistry, University of California at Los Angeles, Los Angeles, California; and †Department of Chemical Engineering, University of California, Santa Barbara, California

ABSTRACT This paper article outlines the results from a combined experimental and theoretical study on the properties of circular domains in a mixed Langmuir monolayer at thermodynamic equilibrium. The mixed monolayer consisted of a binary mixture of dimyristoyl-phosphatidyl-choline and dihydrochloesterol. A long-term fluorescence microscopy study of these domains was carried out over the course of ~60 h. Image analysis of the domains over time revealed that the domains ripened slowly with increase in mean domain radius and decrease in domain number density. At the end of the measurement, the domains remained polydisperse, and true thermodynamic equilibrium was not reached. Theoretically, collective thermodynamic equilibrium properties such as mean domain size and size distribution were calculated by combining micelle self-assembly theory and the ''equivalent dipole'' model for the self-energy of two-dimensional domains. The calculations predicted existence of finite-sized circular domains at equilibrium. This suggests that equilibrium circular monolayer domains of single- or multicomponent lipids with a finite size distribution should form only at very limited experimental conditions. Both the predicted mean domain size and size distribution are strongly affected by line tension and dipole moment density difference. A comparison between the theoretical and experimental results is made.

INTRODUCTION

Despite the advances made in the study of Langmuir monolayers in recent years, many fundamental questions about the thermodynamic nature of these unique pseudo-two-dimensional (2D) systems remain unresolved. One such question concerns the true thermodynamic equilibrium state of the domains in a two-component monolayer, for instance, the black circular domains observed in the mixed monolayer of dimyristoyl-phosphatidyl-choline (DMPC) and dihydrochloesterol (Dchol) by epifluorescence microscopy (1). Many experimental and theoretical investigations have been carried out by McConnell and co-workers on the properties of this mixed monolayer system (for a comprehensive review, see McConnell (2)). It is this body of work that serves as the foundation for the study reported in this article.

Extensive experimental studies have been done on the DMPC/Dchol mixed monolayer to investigate the domain size, size polydispersity, and domain shape (3–6). The phase diagram of the mixed monolayer contains a fluid-in-fluid phase regime where the two components exhibit partial miscibility in the domains and surrounding monolayer (5). Within this regime, circular domains ranging in size from microns to tens of microns have been observed by fluorescence microscopy. An interesting question arises as to whether the monolayer in this regime is a one- or two-phase system, and the answer depends on whether the domains can be considered to be 2D micelles or ''solute aggregates'' in a monolayer ''solvent''—in the latter case, it is a one-phase system regardless of the size of the domains. If the domains are slowly growing until they merge into a single domain, then the system is two-phase. The fundamentally important experimental issue, therefore, is whether these finite-sized domains are stable at equilibrium. Investigation on this issue may also shed light on our understanding of domain and ''raft'' formation in planar biological membranes and vesicles (7–9).

The DMPC/Dchol domains are seen to nucleate and grow after a rapid surface-pressure quench (1,5,6). The latter stages of the growth process follow a modified Ostwald ripening mechanism where the mean domain radius was observed to increase with time t as t^n, where $n \approx 0.28$ (1). The domains ripen with the larger domains growing at the expense of the smaller domains. However, the domains remain polydisperse during their long-term growth (1). Computer simulations of Ostwald ripening of 2D droplets (monolayer domains) under competing interactions have predicted that the growth rate is very slow. Such systems may therefore never reach their true thermodynamic equilibrium state during normal experimental timescales (10–14), because prolonging these times can lead to impurity build-up at the surfaces, which is very difficult to detect. In addition, unlike three-dimensional (3D) systems where buoyancy force enhances droplet coalescence, no such additional ''rate-enhancing'' forces are present in the monolayers.

The shape and size of the DMPC/Dchol domains are determined by the opposing forces of line tension acting at the domain boundary and electrostatic (dipolar or double-layer) interactions between the molecules within each domain. According to the ''equivalent dipole model'' proposed by McConnell et al. (2,15), the molecular interaction energy of an isolated circular domain of radius R, composed of

Submitted January 12, 2006, and accepted for publication April 3, 2006.
Address reprint requests to Yufang Hu, E-mail: yufang_hu@hotmail.com.

0006-3495/06/07/444/10 $2.00
doi: 10.1529/biophysj.106.081000

molecular dipoles that are oriented perpendicular to the air-water interface, is

$$E = 2\pi R\left[\lambda - \frac{m^2}{4\pi\varepsilon\varepsilon_0}\ln\frac{4R}{e^2\Delta}\right], \quad (1)$$

where λ is the line tension and is typically $\lambda \approx 10$ pN. For a monolayer domain whose hydrocarbon thickness is $\Delta\ell$ larger or smaller than that of the surrounding monolayer, the line tension would be $\lambda = \gamma\Delta\ell$, where $\gamma \approx 25$ mJ/m^2 is the surface energy of the hydrocarbon-air interface. For $\Delta\ell = 4$ Å, this gives $\lambda \approx 1.0 \times 10^{-11}$ J/m or 10 pN. Typically measured values are 1–20 pN. m is the dipole moment density difference between the dipolar lipids in the domain and those from the surrounding area, expressed in units of C $\cdot$ m/m^2 = C/m, $\varepsilon_0 = 8.854 \times 10^{-12}$ C^2/J$\cdot$m is the permittivity of free space, ε is the dielectric constant of water, and Δ is the molecular cut-off distance between neighboring dipoles inside the domain and is on the order of a molecular dimension. If N is the number of lipids per domain, each occupying an area a, then $aN = \pi R^2$. The energy per molecule is therefore:

$$\frac{E}{N} = \frac{2a}{R}\left[\lambda - \frac{m^2}{4\pi\varepsilon\varepsilon_0}\ln\frac{4R}{e^2\Delta}\right]. \quad (2)$$

An analogy can be drawn between the concept of the two ''opposing forces'' expressed in Eq. 2 and that introduced by Tanford (16) in his analysis of 3D surfactant micelles. For the 2D monolayer, the line tension plays an analogous role as the interfacial tension in 3D, and acts to reduce the domain boundary and favors macroscopic phase separation of the monolayer. The electrostatic interactions of the vertically oriented dipole are repulsive in nature and favor the dispersion of molecules from each other. This effect is similar to the electrostatic repulsion of the charged surfactant headgroups in the case of the 3D micelles. Similarities can also be drawn between the mixed monolayer and the quasi-2D domains found in ferrofluids, where the competing interactions of magnetic moments and line tension control the domain morphology (17).

By minimizing E/N with respect to R, one obtains the radius R_M of lowest interaction energy per molecule or mole (2,15):

$$R_M = \frac{e^3\Delta}{4}\exp\frac{4\pi\varepsilon\varepsilon_0\lambda}{m^2}. \quad (3)$$

This corresponds to a minimum energy per molecule of

$$\left(\frac{E}{N}\right)_{\min} = \frac{-2am^2}{\pi\varepsilon\varepsilon_0 e^3\Delta}\exp\frac{-4\pi\varepsilon\varepsilon_0\lambda}{m^2}, \quad (4)$$

where the reference state of zero energy, $(E/N) = 0$, is the infinite domain.

McConnell and co-workers postulated that Eq. 3 gives the equilibrium domain radius. Further, it was speculated that at equilibrium the distribution of domain size could be monodisperse or polydisperse at equilibrium (18,19). However, the above analysis does not take into account the total concentration of molecules in the system and their entropy of mixing at the temperature T of the system. Furthermore, experiments have suggested that the equilibrium domain size for certain monolayer systems, such as the DMPC/Dchol mixed monolayer studied here, are large, exceeding micrometers in size (1,18,20). Since for large, micron-sized domains $R_M \gg \Delta$, it is clear that the exponential term in Eq. 3 must be very large. Thus, a small difference in λ or m can have a big effect on R_M. In view of the highly delicate balance between the opposing forces, it is the goal of this study to carry out a full equilibrium thermodynamic analysis of the mixed monolayer system, incorporating parameters such as temperature and amphiphile concentrations into our calculations.

This article presents our attempt to address the issue of equilibrium monolayer domain morphology using a combined experimental and theoretical approach. It is organized as follows: first, results from a long-time fluorescence microscopy study of the evolution of circular domains are presented, which is followed by a theoretical analysis of equilibrium domain morphology. The theoretical analysis combines the ''equivalent dipole model'' by McConnell et al. with the theory for the self-assembly of amphiliphic molecules by Tanford (16) as extended by Israelachvili et al. (21,22) to nonspherical micelles and vesicles and, later, to the pressure-area (Π-A) isotherms of monolayers containing small 2D micelles (23).

EXPERIMENTAL METHODS

Materials

1,2-Dimyristoyl-*sn*-glycero-3-phosphocholine was purchased in powder form from Avanti Polar Lipids (Birmingham, AL). Dchol was purchased from Sigma (St. Louis, MO). The fluorescent dye 1,2-dihexadecanoyl-*sn*-glycero-3-phosphoethanolamine, triethylammonium salt (Texas Red PE) was purchased from Molecular Probes (Eugene, OR). All chemicals were used without further purification. A chloroform spreading solution with DMPC/DChol/Texas Red PE molar ratios of 89.5%:10%:0.5% was used in all experiments.

Preparation and imaging of the monolayer

The water used for the monolayer subphase was purified by a MiliPore Gradient A10 system (Bedford, MA), producing water with a resistivity of $\geq$18.2 MΩ cm and total organic content of $\leq$5 ppb. A Pyrex glass Petri dish (diameter 10.2 cm) was used in place of a conventional Langmuir trough. This allowed the water surface to remain flat right up to the glass surface rather than curving at the Teflon surfaces of the trough walls, which causes unwanted buoyancy and curvature effects on the domains. The Pyrex Petri dish was cleaned by soaking in a solution of isopropanol saturated with potassium hydroxide, followed by extensive rinsing with Milli-Q water.

At the beginning of each experiment the freshly cleaned Petri dish was filled with Milli-Q water and the lipid spreading solution was evenly deposited on the surface. The amount of lipid deposited was calculated according to the Langmuir isotherm (24) and the published phase diagram

(24) so that the resultant monolayer was in the fluid-in-fluid regime. The monolayer surface pressure was ~2 mN/m. The monolayer was discarded if nonuniform features such as stripes, foam structures, or a dark patch containing irregular structures were observed. Video recordings of the monolayer were done at regular time intervals. For each recording, multiple images at different parts of the monolayer were taken for statistical purposes. To prevent contamination and water evaporation, the Petri dish was capped with a glass cover throughout the experiment. The cover was replaced with a piece of indium-tin-oxide-coated glass during imaging. A low current was passed through the indium tin oxide layer to eliminate water condensation on the glass. All experiments were conducted at 23 ± 1°C.

All imaging was performed on a Nikon Eclipse fluorescent microscope (Melville, NY). The fluorescence images from the microscope were fed to a Cohu image-intensified CCD camera (San Diego, CA) that was directly connected to the microscope. The fluorescence images were recorded using a JVC DV-SVHS VCR in Super VHS mode (Cypress, CA). Video images were played back on a PC installed with AGP4 64MB TV card (ATI Technologies, Ontario, Canada). VirtualDub 1.4.10 software was used for frame capture from the video. The captured images were processed and analyzed using Scion Image for Windows Beta 4.0.2 (Scion Corp., Frederick, MD).

EXPERIMENTAL RESULTS

Time evolution of domain size

Fluorescence images of the domains and their size distribution and mean domain size as functions of time from a typical experiment are shown in Fig. 1. The experiment was terminated 64 h after the initial monolayer deposition, when the monolayer became contaminated and the domain morphology became irregular. During this time window, the mean domain size increased over time (Fig. 1, *a* and *c*), whereas size distribution remained polydisperse (Fig. 1 *b*). The rate of increase of the domain size was very slow. The system did not reach thermodynamic equilibrium during the experimental time window as both the mean domain radius and the domain size polydispersity were still changing at the point of the last measurement. The domains evolved via the classic Ostwald ripening scheme, in which the larger domains grow at the expense of the smaller domains (1). Qualitatively similar results were obtained when the monolayer was spread on an environmentally sealed miniature trough (20) and these results agreed with data published by Seul and co-workers (25–27), where a thorough analysis of the domain coarsening kinetics was made. In these studies, the monolayer domain growth was monitored following a rapid pressure quench from a homogeneous one-phase state to a fluid-in-fluid regime.

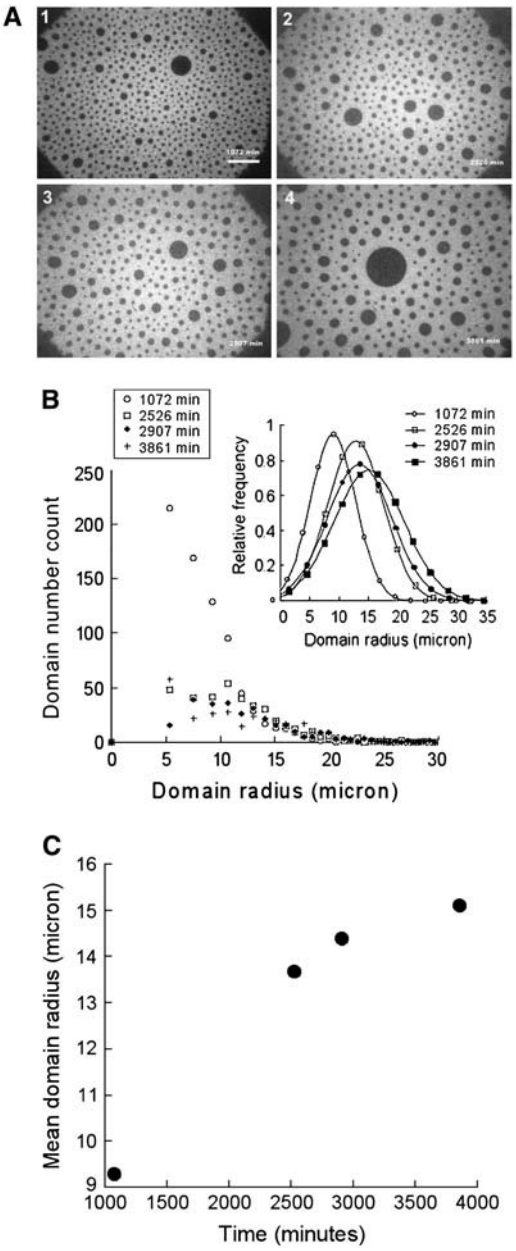

FIGURE 1 (*a*) Fluorescence images of the monolayer taken at (*1*) 1072, (*2*) 2526, (*3*) 2907, and (*4*) 3861 min after monolayer spreading. Scale bar, 100 μm. (*b*) Domain size distribution of the monolayer measured at the four time intervals between 0 and 3861 min. The insert shows the Gaussian fits to the normalized domain size distribution. The number count was taken over the entire view, as shown in *a*. Thus, all counts were taken over a fixed area of monolayer. (*c*) Mean domain radius as a function of time. The first data point was taken at 1072 min after monolayer spreading. For earlier times, the domains were too small to be analyzed accurately.

THEORY BACKGROUND

Theory of 2D self-assembled aggregates

The standard theory for the self-assembly of amphiphilic molecules by Hill (28), Hall and Pethica (29), Tanford (16), and Israelachvili et al. (21,22,30) can be applied to calculate the mean size and size distribution of 2D monolayer domains. The theory combines solution thermodynamics with a phenomenological description of the molecular interaction energies, and gives a set of equations for determining the equilibrium aggregate size distribution. For a dilute one-component system, the distribution is given by (31)

$$X_N = N\{X_1 \exp[(\mu_1^0 - \mu_N^0)/kT]\}^N, \quad (5)$$

where X_N is the concentration of molecules in aggregates of aggregation number N; and μ_N^0 is the mean interaction free energy per molecule in these aggregates. This molecular free energy function μ_N^0 contains the total mean molecular interaction per molecule with all the other molecules in the aggregate, with the surrounding solvent and, for more concentrated systems where interaggregate interactions are significant, with molecules in nearby aggregates. If the aggregation number peaks around a mean value M, rearrangement of Eq. 5, using M as a reference state, leads to a more convenient expression about the concentration of aggregate of size N (31):

$$X_N = N\{X_M/M \exp[M(\mu_M^0 - \mu_N^0)/kT]\}^{N/M}. \quad (6)$$

To apply the theory to the mixed monolayer system, the mixed monolayer of DMPC and Dchol is modeled as a 2D binary fluid mixture (Fig. 2). The phase diagram of the monolayer has been established experimentally (5,24) and consists of a phase boundary separating the homogeneous one-phase regime and a fluid-in-fluid phase regime. We will demonstrate in the following sections that this pseudo phase coexistence regime is essentially a one-phase regime containing homogeneously distributed domains with a finite size distribution. Within the pseudo two-phase coexistence regime, the compositions of the two microphases are approximated by the lever rule (24).

The two microphases in this pseudo two-phase regime are the experimentally observed black circular domains rich in DChol (the black phase), and the homogeneous white background rich in DMPC (the white phase), as shown in Fig. 1. Within the pseudo two-phase regime the mixed monolayer is treated as composed of the homogeneous background (solvent) and the self-assembled circular domains (solute). The formation of the circular domains is driven by the competing interactions of line tension at the domain boundary and the DMPC headgroup dipole-dipole repulsion (Fig. 2). The experimentally observed number density of these circular domains was low, as was the total area fraction of the black phase (cf. Fig. 1). Therefore, the interdomain interactions are assumed to be weak. Each domain is effectively a giant dipole and the domains remain separated from each other due to their weak long-range dipole-dipole repulsion. Ideal mixing is assumed for all domains in a monolayer, as well as for molecules within each domain. Parallel to the experiments, for a monolayer at equilibrium with fixed temperature and overall molar composition, the only degree of freedom in our calculations is the monolayer surface pressure.

Following these assumptions, a set of basic equations describing the energy and material balances of the mixed monolayer system can be written. The energy of a circular domain is given by Eq. 1. For an isolated circular domain composed of N DMPC molecules (Fig. 2), let the apparent cross-sectional area of each DMPC molecule be a. Then,

$$R = \left(\frac{aN}{\pi}\right)^{1/2}. \quad (7)$$

Since each circular domain contains DMPC as well as Dchol molecules, the apparent cross-sectional area a defined in Eq. 7 contains contributions from both types of molecules. More details on the estimation of a are given in the next section.

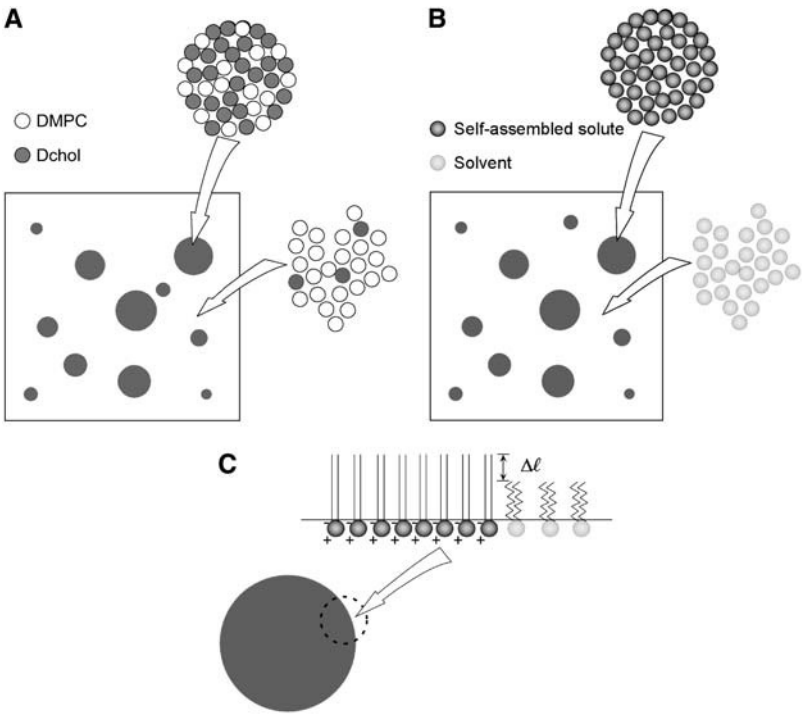

FIGURE 2 Schematic of the 2D self-assembly model. (*a*) A simplified view of the mixed DMPC/Dchol monolayer in the pseudo two-phase regime. The circular domains are Dchol-rich and the white background is DMPC-rich. (*b*) The mixed monolayer in view of the ''equivalent dipole model''. The circular domains (aggregates) are formed by self-assembled solute molecules in a background of homogenous solvent. The self-assembly of the solute molecules is driven by line tension and dipole-dipole repulsion. The compositions of the aggregates are calculated by imposing energy and material constraints. (*c*) The model used to calculate line tension, which is proportional to the hydrocarbon chain length mismatch at the domain boundary.

Combining Eqs. 1 and 7 and adding the entropy of mixing of the DMPC and Dchol molecules within a domain gives the mean interaction free energy per domain or per aggregate at equilibrium as a function of domain size N:

$$E = \frac{2\sqrt{\frac{aN}{\pi}}\left[4\varepsilon\varepsilon_0\pi\lambda + m^2\ln\left(\frac{\sqrt{\pi}\Delta e^2}{4\sqrt{aN}}\right)\right]}{2\varepsilon\varepsilon_0} + \frac{N}{X_{\text{DMPC\_black}}}k_BT\left(X_{\text{DMPC\_black}}\ln X_{\text{DMPC\_black}} + X_{\text{Dchol\_black}}\ln X_{\text{Dchol\_black}}\right), \quad (8)$$

where $X_{\text{DMPC\_black}}$ and $X_{\text{Dchol\_black}}$ are the mole fractions of DMPC and Dchol, respectively, in the black phase and

$$X_{\text{Dchol\_black}} + X_{\text{DMPC\_black}} = 1. \quad (9)$$

The entropy of mixing of the DMPC-rich white phase is negligible compared with that of the black phase, thus it is not included in Eq. 8. The molecular cut-off distance Δ in Eq. 8 is taken to be 5 Å, which is the value used by McConnell et al. (15).

The mean interaction free energy per molecule in an aggregate of size N is obtained from Eq. 8:

$$\mu_{\text{N}}^0 = (E/N) = \frac{a\left[4\varepsilon\varepsilon_0\lambda\pi + m^2\ln\frac{\Delta\sqrt{\pi}e^2}{4\sqrt{aN}}\right]}{2\varepsilon\varepsilon_0\sqrt{aN\pi}} + \frac{k_{\text{B}}T}{X_{\text{DMPC\_black}}}\left(X_{\text{DMPC\_black}}\ln X_{\text{DMPC\_black}} + X_{\text{Dchol\_black}}\ln X_{\text{Dchol\_black}}\right). \quad (10)$$

The reference state M in Eq. 6 is chosen to correspond to the minimum of the molecular free energy, μ_{M}^0:

$$N\Big|_{\frac{\partial\mu_{\text{N}}^0}{\partial N}=0} = M. \quad (11)$$

Finally, all the DMPC molecules in the black phase obey the material balance:

$$\sum_{\text{N}=1}^{\infty} X_{\text{N}} = X_{\text{DMPC\_black}} \times B, \quad (12)$$

and

$$B + W = 1. \quad (13)$$

B and W are the total mole fractions of the black and white phases; and X_{N} is given by Eq. 6.

The size distribution of aggregates is calculated by solving Eqs. 6, 10, and 12 simultaneously.

Models of line tension and dipole moment density difference

As evident from Eqs. 1 and 3, the line tension λ and the dipole moment density difference m are two key parameters in determining the molecular free energy μ_{N}^0, and, subsequently, the mean equilibrium domain size R_{M}. By definition, m is given as

$$m = \mu_{\text{DMPC\_black}}/a_{\text{DMPC\_black}} - \mu_{\text{DMPC\_white}}/a_{\text{DMPC\_white}}, \quad (14)$$

where $\mu_{\text{DMPC\_black}}$ and $\mu_{\text{DMPC\_white}}$ are the dipole moments in the black and white phases, respectively, and are both taken to be 24 Debye, and $a_{\text{DMPC\_white}}$ and $a_{\text{DMPC\_black}}$ are the area per DMPC molecule in the two respective phases. The dipole moments $\mu_{\text{DMPC\_black}}$ and $\mu_{\text{DMPC\_white}}$ are calculated by assuming that only the ziwitterionic DMPC molecules carry dipoles. Further, the dipole on each DMPC molecule is localized on its headgroup with the separation distance between the charges comparable to the size of the headgroup, which is 5 Å. The value of m was measured at several fixed monolayer compositions and surface pressures (24,32,33). By establishing m as a function of area per lipid molecule, our model takes into account the variation of m with monolayer surface pressure. The line tension as a function of surface pressure is calculated using a simple model illustrated in Fig. 2. Specifically, the line tension is proportional to the DMPC hydrocarbon chain mismatch between the black and white phases:

$$\frac{\lambda_1}{\lambda_2} = \frac{\Delta\ell_1}{\Delta\ell_2}, \quad (15)$$

where $\Delta\ell$ is defined as the height difference of DMPC molecules in the two phases:

$$\Delta\ell = \ell_{\text{DMPC\_black}} - \ell_{\text{DMPC\_white}}. \quad (16)$$

The reference line tension at $\Pi = 2$ mN/m was assigned a value of $\lambda = 7$ pN, from which all other line tension values are inferred. Assuming the volume of a DMPC molecule is constant at 800 Å^3 (31), $\Delta\ell$ can be calculated once $a_{\text{DMPC\_white}}$ and $a_{\text{DMPC\_black}}$ are known.

The areas per DMPC molecule in the two phases as a function of surface pressure are calculated from empirical data (3,24). For the white phase:

$$a_{\text{DMPC\_white}} = \frac{A_{\text{white}}}{X_{\text{DMPC\_white}} \times W}, \quad (17)$$

where A_{white} is the total area of the white phase and $X_{\text{DMPC\_white}}$ is the mole fraction of the DMPC. Further,

$$X_{\text{DMPC\_white}} + X_{\text{Dchol\_white}} = 1. \quad (18)$$

The component mole fractions $X_{\text{DMPC\_white}}$ and $X_{\text{Dchol\_white}}$ are obtained from empirical phase diagram (24) and observe the following relations:

$$X_{\text{DMPC\_white}} \times W + X_{\text{DMPC\_black}} \times B = 0.9, \quad (19)$$

and

$$X_{\text{Dchol\_white}} \times W + X_{\text{Dchol\_black}} \times B = 0.1. \quad (20)$$

The overall mole fractions of DMPC and Dchol are 90% and 10%, respectively—in accordance with the experimental conditions.

The black phase is highly enriched in Dchol, which forms complexes with DMPC and causes the hydrocarbon chains of the latter molecule to be in an ''entropically extended'' state (Fig. 2) (31,34). As a result, in contrast to the white phase, the DMPC molecules in the black phase are relatively rigid and far less compressible. The hydrocarbon chain length of the DMPC molecules in the black phase is assumed to be insensitive to the monolayer surface pressure change. Consequently, the area occupied per DMPC molecule in the black phase remains constant. For the DMPC molecules in the black phase, the total length of the DMPC molecules with the headgroup plus the hydrocarbon chains is taken to be $\ell = 20$ Å; and the apparent area per DMPC headgroup is $a_{\text{DMPC\_black}} = 50$ Å^2.

CALCULATION RESULTS

Evaluation of the system parameters

To facilitate comparison of the calculation results and experimental measurements, experimental values were used in our calculations whenever possible. Analyses were carried out for three surface pressure values at $\Pi = 2, 4$, and 6 mN/m, which are far below the experimentally measured phase transition point (24). At each surface pressure, the compositions of the black and white phases were calculated using the scheme outlined above. Table 1 lists the compositions of the black and white phases calculated from Eqs. 19 and 20.

The area per DMPC and Dchol molecules in the two phases were calculated using Eqs. 17–20. From these values, the dipole moment density difference, m, and the line tension, λ, were obtained.

The dipole moments of amphiphiles in monolayers at the air-water interface is a function of the dielectric constant ε, which is determined by the location of the amphiphile relative to the interface. As demonstrated by Andelman et al. (35), the effective dipole moments, which point perpendicular to the interface in the ''equivalent dipole model'', are given by $\mu^2_{\text{effective}} = \mu^2_{\text{vacuum}}\epsilon_{\text{air}}/\epsilon_{\text{medium}}(\epsilon_{\text{medium}}+\epsilon_{\text{air}})$. When the amphiphile headgroups are completely immersed in the water phase, $\epsilon_{\text{medium}} = \epsilon_{\text{water}} = 80$, giving $\mu^2_{\text{effective}} = \frac{1}{6400}\mu^2_{\text{vacuum}}$. On the other hand, if the amphiphile headgroups are completely in air, $\mu^2_{\text{effective}} = \frac{1}{2}\mu^2_{\text{vacuum}}$. Since the air-water interface is in reality rather diffuse, the exact location of the amphiphile molecules are difficult to pinpoint. However, experimentally measured m values such as those from surface potential measurements, which are taken to include the contributions from the local dielectric constants, give the ''correct'' values to be used in the above equations.

TABLE 1 Compositions of black and white phases at equilibrium

Π (mN/m)	W (mole fraction)	B (mole fraction)	$X_{\text{DMPC\_white}}$ (mole fraction)	$X_{\text{DMPC\_black}}$ (mole fraction)
2	0.88	0.12	0.97	0.39
4	0.90	0.10	0.95	0.46
6	0.92	0.08	0.93	0.53

TABLE 2 Dipole moment density difference m, and line tension λ at equilibrium

Π (mN/m)	m (Debye/nm^2)	λ (pN)
2	24.8	7.0
4	23.5	6.7
6	22.0	6.5

Mean interaction free energy per molecule in the aggregate

The line energy, dipolar energy, and the complete molecular free energy as functions of aggregate size N for $\Pi = 2$ mN/m are shown in Fig. 3. The constant intradomain entropy of mixing, which is the dominant term in the aggregate-forming regime, is not plotted. The shape of the μ^0_N curve is determined by the interaction energy term in Eq. 10, which is composed of line and dipolar energies. The μ^0_N curve reaches a

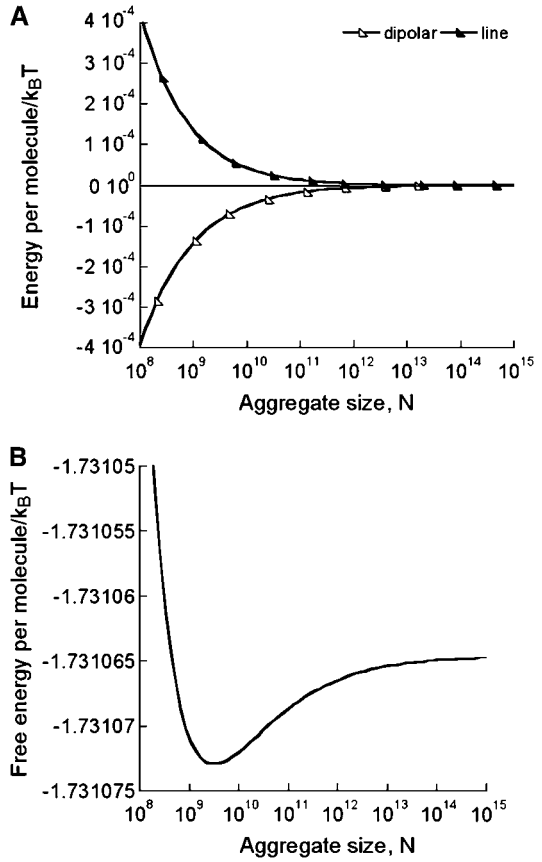

FIGURE 3 The breakdown of the molecular free energy μ^0_N. The minimum in the free energy is the result of the opposing interactions of line tension and dipole-dipole repulsion. The intradomain entropy of mixing is constant in regard to the aggregate size and is not shown. (*a*) The line and dipolar energies. (*b*) The molecular free energy μ^0_N plotted on the same scale as *a*.

minimum value at a finite value of N and asymptotes to a constant value as N approaches infinity. The value of μ_N^0 rises rapidly for small N. Analogous to the formation of surfactant micelles in 3D (31) and other ''supramolecular polymer systems'' (36) where the stable, finite size aggregate forms near the energy minimum, the presence of an energy minimum such as the one shown in Fig. 3 is a necessary but not sufficient condition for the formation of thermodynamically stable aggregates. Qualitative features of these 2D aggregates can be deduced from the shape of the free energy curve: the formation of very small domains is energetically costly and thus prohibited. However stable, finite-sized domains may form as a result of the balance between attractive line tension and repulsive dipole-dipole interactions.

Both the line and dipolar energy are functions of the area per DMPC molecule in the monolayer. Therefore, both quantities are subject to surface pressure changes. This is shown in Fig. 4, where these two component energies are plotted against aggregate size for different surface pressures. Both the line and dipolar energies diminish as the aggregate size grows. Upon surface pressure increase, the DMPC molecules in the white phase are compressed, and their hydrocarbon chains more extended, leading to a reduction of the line tension and the dipole moment density difference. As seen in Fig. 4, when surface pressure increases from 2 to 6 mN/m, changes in the dipolar energy slightly outpace that in line tension, which leads to a shift of the minimum of μ_N^0 curve toward higher values (Fig. 5). The value of the minimum M as defined in Eq. 11 appears to be sensitive to small perturbations in surface pressure: when the surface pressure is increased by 4 mN/m, the value of M increases from 3.2×10^9 to 8.5×10^{10}. Such a dramatic shift in the free energy minimum is a reflection of the delicate balance of the competing interactions of line tension and dipolar repulsion.

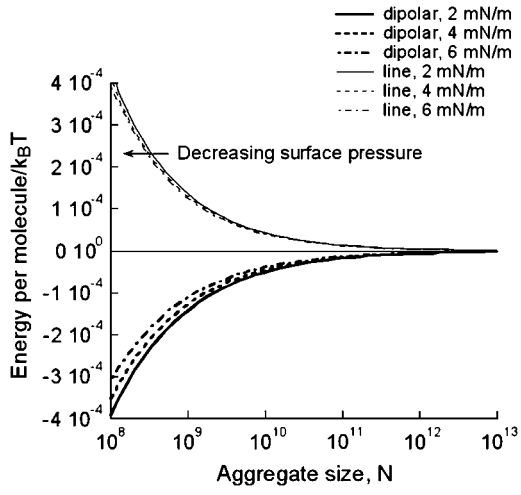

FIGURE 4 Line and dipolar energies as functions of surface pressure. The change in dipolar energy slightly outpaces that of the line energy.

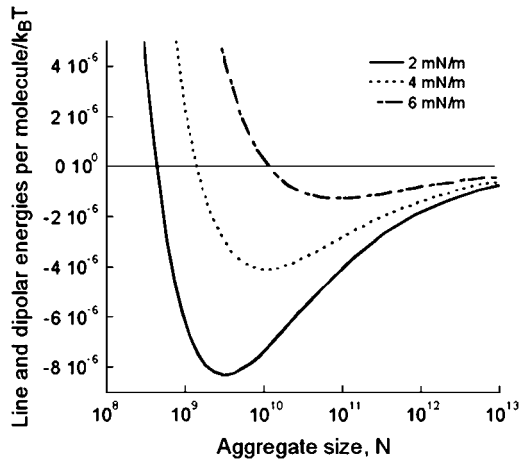

FIGURE 5 Sum of the line and dipolar energies by Eq. 10 as a function of domain aggregation number N at different surface pressures. The reference state M, as determined by the minimum of the energy sum (the entropy-of-mixing term in Eq. 10 is constant with respect to domain size), shifts to a higher aggregation number with increasing surface pressure.

Domain size distribution and mean domain size

The mean aggregate size and domain size distribution are obtained by solving Eqs. 6, 10, and 12 simultaneously. Convergence of results, when both the material and energy constraints are satisfied, are obtained for $\Pi = 2$, 4, and 6 mN/m. The resulting aggregate size distribution curves are plotted in Fig. 6, where the aggregate mole fraction X_N is given by Eqs. 6 and 12. The distribution curves are shifted horizontally to overlap. All three distribution curves appear symmetrical around a mean domain size $\overline{N}$ with the maxima of the peaks highly sensitive to surface pressure. The broadening of the size distribution curve at higher surface pressure is manifested as the increase in the standard deviation in the domain size distribution δ, which is defined as

$$\delta^2 = \frac{\sum_{N=1}^{\infty} N^2 X_N}{\sum_{N=1}^{\infty} X_N} - \overline{N}^2, \tag{21}$$

where the mean domain size $\overline{N}$ is

$$\overline{N} = \frac{\sum_{N=1}^{\infty} N X_N}{\sum_{N=1}^{\infty} X_N}. \tag{22}$$

The calculated values of δ for $\Pi = 2$, 4, and 6 mN/m are 3.9×10^7, 1.0×10^8, and 5.2×10^8, respectively. The ratios of $\delta/\overline{N}$, which are measures of ''normalized'' domain size polydispersities for $\Pi = 2$, 4, and 6 mN/m, are 1.23%, 0.96%, and 0.61%, respectively. Thus, as the surface

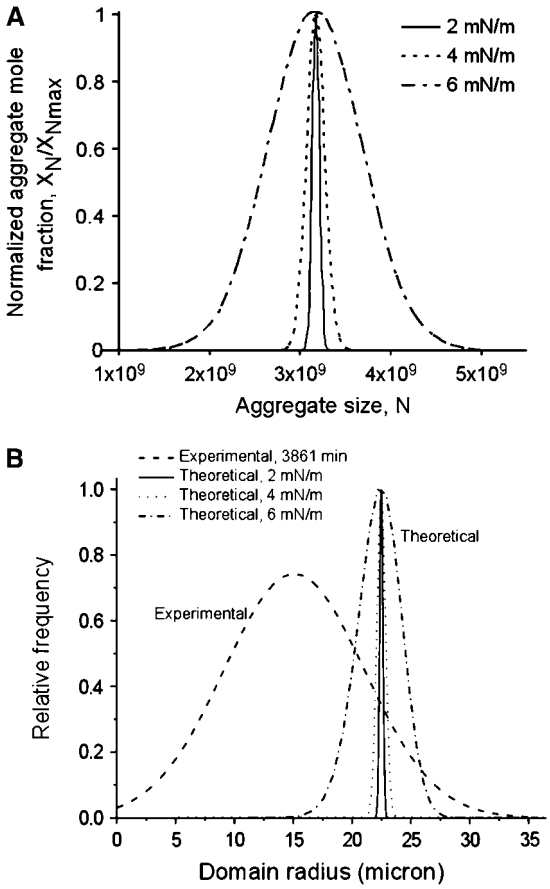

FIGURE 6 Domain size distribution as a function of surface pressure. The distribution curves become broader as surface pressure is increased. The size distribution curves are normalized against the peak heights. For $\Pi = 2$, 4, and 6 mN/m, the maximum distributions occur around $X_{Nmax} = 4.1\times10^{10}$, 1.7×10^{10}, and 3.0×10^{-11} mole fractions, respectively. (*a*) The normalized size distribution plotted against aggregate size *N*. (*b*) Comparison between the predicted normalized size distribution and the Gaussian fit of the measured distribution at $t = 3861$ min. The domain radii are calculated by $aN = \pi R^2$, where *a* is the apparent area per DMPC headgroup in the black phase and is equal to 50 Å^2. Note that the predicted distributions are much sharper than the measured distribution.

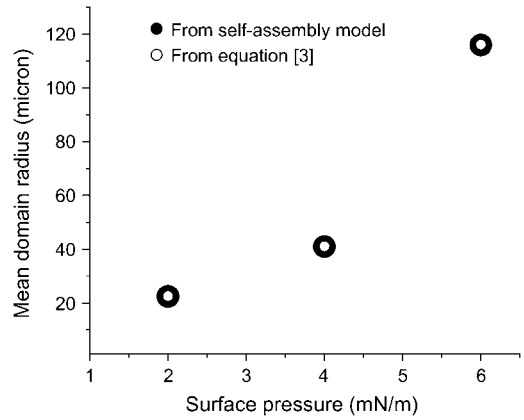

FIGURE 7 Mean domain radius as a function of surface pressure. The difference between radii calculated using the self-assembly scheme and Eq. 3 is <1% for $\Pi = 2$, 4,and 6 mN/m.

pressure increases, the domain size polydispersity decreases. A comparison of the Gaussian curve fit of the experimentally measured domain size distribution at $t = 3861$ min to the normalized theoretical size distribution (cf. Figs. 1 *b* and 7 *a*) are given in Fig. 7 *b*. The theoretical curves at $\Pi = 4$ and 6 mN/m are shifted horizontally to overlap with that at $\Pi = 2$ mN/m. Comparison of the experimental and theoretical mean domain size and the domain size polydispersity indicate that the monolayer at the time of the last measurement was still evolving toward equilibrium; and that the theoretical size distributions are much narrower than the experimentally measured distributions at different surface pressures. For the mixed monolayer of DMPC/Dchol, the equilibration rate toward the final equilibrium state may be very slow, as estimated by others (1,19). Further, during the equilibration process the system may be kinetically trapped in various metastable states (37). Therefore, it is very likely that the equilibrium state may not be experimentally accessible due to technical constraints such as amphiphile decomposition or contamination over time.

The mean aggregate size $\overline{N}$ falls slightly lower than the reference state *M* at all three surface pressures, whereas *M* never exceeds $\overline{N}$ by >1%. The smaller value of $\overline{N}$ is due to the incorporation of the entropies of mixing both within each domain and among different domains. This suggests that for the present system, the effect of entropy on mean domain size is small, since $\overline{N}$ is calculated essentially from *M* by adding the effect of entropy. A small perturbation in surface pressure causes a large shift in the value of $\overline{N}$: the mean domain size at 6 mN/m is more than a factor of 20 larger than at 2 mN/m.

In view of the small contribution of entropies to the equilibrium mean domain size $\overline{N}$, as suggested by the above analysis, it is worthwhile to compare the equilibrium mean domain size calculated from the self-assembly theory to that obtained directly from Eq. 3, which does not contain the effect of entropy. A comparison of these two sets of values as functions of surface pressure is shown in Fig. 7. The conversion from mean aggregate number to mean domain radius is done by letting $aN = \pi R^2$, with $a = 50$ Å^2. When the surface pressure is increased from 2 to 6 mN/m, the mean domain radius calculated by both methods grows from ~22.5 to 116.0 μm. However, the difference between the radii calculated using these two methods is <1% at all surface pressures.

The largest measured mean domain radius was 15.1 μm at $t = 3861$ min, which is lower than the smallest predicted mean radius of 22.5 μm at 2 mN/m. Although the surface pressure was unknown in our experiment, we believe it was higher than 2 mN/m based on calculation of the average area/molecule at monolayer deposition. Subsequently, the equilibrium domain radius at our experimental condition should be ≥22.5 μm. Although a true equilibrium state was not

reached experimentally and the domains were still ripening at $t = 3861$ min, the measured domain size of 15.1 μm provides an estimate of the lower bound of the equilibrium radius.

The above calculation results predict that within a narrow range of surface pressures, macroscopic circular domains like those observed experimentally exist at equilibrium with a finite size polydispersity. Our calculations do not assume that these domains are distributed on any geometric lattice, and their spatial distribution is random with the unique size distribution preserved throughout the entire surface of the monolayer, and as such, the mixed monolayer is essentially a one-phase system.

DISCUSSION

It is important to address the distinction between the self-assembly theory and the models of macroscopic materials balance, line tension, and dipole moment density difference used in our calculations. The self-assembly theory as originally derived for 3D micelle self-assembly has been applied to other self-assembled systems such as lipid bilayers, lipid vesicles, and monolayers (22,30,38–40). Its applicability to the present system of domains in the binary mixed monolayer is based on the assumptions that the 2D mixed monolayer is an ideal solution mixture, and that the concentration of the domains within the monolayer is low, so there is no interaction between different domains. When these assumptions are valid, this formalism can be extended to calculate the properties of aggregates formed in other surface pressure regimes, such as the gaseous regime at very low surface pressures (40), or alternatively to the high-surface-pressure regime near the critical miscibility point, where the circular domain shape first becomes unstable and eventually disappears. Thus, the self-assembly theory can be applied to treat other self-assembled systems so long as the above listed assumptions are satisfied. The models of materials balance, line tension, and dipole moment density difference, on the other hand, are restricted to the current system of DMPC/Dchol mixed monolayer only. Moreover, the validity of the models is limited to a certain surface-pressure range, and far away from the critical miscibility point, because near the critical miscibility point, properties such as line tension and dipole moment density difference become highly nonlinear with respect to surface pressure. A thorough investigation of the surface pressure dependence of these properties is beyond the scope of this study. The models of line tension and dipole moment density difference are restricted to homogeneous circular domains, and therefore are not applicable to the gaseous regime, where the domain morphology is much more complicated.

Our attempt at prolonged experimental study on the equilibration process of circular 2D domains of DMPC/Dchol monolayer has demonstrated that the slow ripening rate of the system renders the state of thermodynamic equilibrium experimentally inaccessible. Through subsequent theoretical study we attempt to address the equilibrium monolayer properties by applying the theory of self-assembly of 3D micelles and models of macroscopic material balance, line tension, and dipole moment density to the circular domains found in the mixed monolayer. To our knowledge, this is the first time that a full thermodynamic analysis has been applied to the mixed monolayer system by taking into account both the energy and mass constraints. The results from our calculations show qualitative agreement with previous theoretical calculations on equilibrium radius and domain size distributions by other authors (41–43): Namely, the equilibrium domain radius increases at higher surface pressure, whereas the domain size polydispersity decreases. The inclusion of various entropies into our calculations yields a prediction of the domain size polydispersity, which is lacking in interaction energy-only models such as Eq. 3. Unlike surfactant micelle aggregates, where there exists a strong dependence of the mean aggregate size on entropy, which manifests as the strong correlation between mean aggregate size and total amphiphile concentration (21), our calculations show that for the system described here, the effect of entropy on mean domain size is minimal. Application of the self-assembly theory to lipid vesicles has led to a similar conclusion, namely that the mean vesicle size is not strongly affected by the lipid concentration fluctuations (21,22). This suggests that at above the minimum monomer concentration required for aggregate formation (critical aggregate concentration), the mean aggregate size of smaller-sized self-assembled systems such as micelles is more susceptible to thermal fluctuations than are those of larger systems, such as vesicles and monolayer domains.

CONCLUSIONS

The calculations presented in this article have extended the formalism of a full thermodynamic analysis of the 3D self-assembly of surfactant micelles to 2D lipid domains in a binary mixed monolayer. Some fundamental similarities can be found in these two systems: both assembly processes are driven by competing interactions and both systems have Gaussian-like aggregate size distributions at equilibrium. In the micellar case, the aggregate formation is the result of a balance between the headgroup repulsion and hydrocarbon tail attraction, whereas in the monolayer case, it is due to the attractive line tension and dipolar repulsion. The delicate balance between the opposing forces in the monolayer case results in significant shifts in mean domain size and domain size polydispersity following small perturbations on surface pressure. Unlike in the micellar system, the entropy plays a weak role in determination of mean domain size of the monolayer domains. Further, our phenomenological model predicts that at thermodynamic equilibrium, under limited conditions, the monolayer does not macroscopically phase-separate and

stable domains with a finite size distribution exist at thermodynamic equilibrium.

We thank Ka Yee Lee for initiating our interest in this project and for many stimulating discussions; Phil Pincus for helpful discussions on electrostatics, Tom Chou and Roya Zandi for critical comments on the thermodynamics of self-assembly, and Arrelaine Demeron for her assistance with the experimental measurements during her research internships at University of California, Santa Barbara.

This work was partially supported by the MRSEC Program of the National Science Foundation under Award No. DMR05-20415.

REFERENCES

1. Seul, M., N. Y. Morgan, and C. Sire. 1994. Domain coarsening in a two-dimensional binary mixture: growth dynamics and spatial correlations. *Phys. Rev. Lett.* 73:2284–2287.
2. McConnell, H. M. 1991. Structures and transitions in lipid monolayers at the air- water interface. *Annu. Rev. Phys. Chem.* 42:171–195.
3. Benvegnu, D. J., and H. M. McConnell. 1992. Line tension between liquid domains in lipid monolayers. *J. Phys. Chem.* 96:6820–6824.
4. Dekoker, R., and H. M. McConnell. 1994. Shape transitions of lipid monolayer domains in an external field. *J. Phys. Chem.* 98:5389–5393.
5. Hirshfeld, C. L., and M. Seul. 1990. Critical mixing in monomolecular films: pressure-composition phase diagram of a two-dimensional binary mixture. *J. Phys. [E].* 51:1537–1552.
6. Seul, M., and M. J. Sammon. 1990. Competing interactions and domain-shape instabilities in a monomolecular film at an air-water interface. *Phys. Rev. Lett.* 64:1903–1906.
7. Veatch, S. L., and S. L. Keller. 2003. Separation of liquid phases in giant vesicles of ternary mixtures of phospholipids and cholesterol. *Biophys. J.* 85:3074–3083.
8. London, E. 2002. Insights into lipid raft structure and formation from experiments in model membranes. *Curr. Opin. Struct. Biol.* 12:480–486.
9. Edidin, M. 2001. Shrinking patches and slippery rafts: scales of domains in the plasma membrane. *Trends Cell Biol.* 11:492–496.
10. Sagui, C., and R. C. Desai. 1995. Late-stage kinetics of systems with competing interactions quenched into the hexagonal phase. *Phys. Rev. E.* 52:2807–2821.
11. Sagui, C., and R. C. Desai. 1995. Effects of long-range repulsive interactions on Ostwald ripening. *Phys. Rev. E.* 52:2822–2840.
12. Desai, R. C., and C. Sagui. 1995. Kinetics of phase ordering in systems with competing interactions. *J. Magn. Magn. Mater.* 149:87–92.
13. Sagui, C., and R. C. Desai. 1994. Kinetics of phase-separation in two-dimensional systems with competing interactions. *Phys. Rev. E.* 49: 2225–2244.
14. Sagui, C., and R. C. Desai. 1993. Kinetics of topological defects in systems with competing interactions. *Phys. Rev. Lett.* 71:3995–3998.
15. McConnell, H. M., and V. T. Moy. 1988. Shapes of finite wo-dimensional lipid domains. *J. Phys. Chem.* 92:4520–4525.
16. Tanford, C. 1980. The Hydrophobic Effect: Formation of Micelles and Biological Membranes. Wiley, New York.
17. Dickstein, A. J., S. Erramilli, R. E. Goldstein, D. P. Jackson, and S. A. Langer. 1993. Labyrinthine pattern-formation in magnetic fluids. *Science.* 261:1012–1015.
18. McConnell, H. M., and R. DeKoker. 1996. Equilibrium thermodynamics of lipid monolayer domains. *Langmuir.* 12:4897–4904.
19. McConnell, H. M. 1996. Equilibration rates in lipid monolayers. *Proc. Natl. Acad. Sci. USA.* 93:15001–15003.
20. Hu, Y. F., K. Y. C. Lee, and J. Israelachvili. 2003. Sealed minitrough for microscopy and long-term stability studies of Langmuir monolayers. *Langmuir.* 19:100–104.
21. Israelachvili, J. N., D. J. Mitchell, and B. W. Ninham. 1976. Theory of self-assembly of hydrocarbon amphiphiles into micelles and bilayers. *J. Chem. Soc. Faraday Trans.* 72:1525–1568.
22. Israelachvili, J. N., D. J. Mitchell, and B. W. Ninham. 1977. Theory of self-assembly of lipid bilayers and vesicles. *Biochim. Biophys. Acta.* 470:185–201.
23. Israelachvili, J. 1994. Self-assembly in two dimensions: surface micelles and domain formation in monolayers. *Langmuir.* 10:3774–3781.
24. Benvegnu, D. J., and H. M. McConnell. 1993. Surface dipole densities in lipid monolayers. *J. Phys. Chem.* 97:6686–6691.
25. Seul, M. 1994. Stripe-to-droplet transition in an organic monolayer: quenched connectivity. *Europhys. Lett.* 28:557–563.
26. Sire, C., and M. Seul. 1995. Maximum entropy analysis of disordered droplet patterns. *J. Phys. I.* 5:97–109.
27. Morgan, N. Y., and M. Seul. 1995. Structure of disordered droplet domain patterns in a monomolecular film. *J. Phys. Chem.* 99:2088–2095.
28. Hill, T. L. 1963, 1964. Thermodynamics of Small Systems. W. A. Benjamin, New York.
29. Hall, D. G., and B. A. Pathica. 1967. *In* Nonionic Surfactants. M. J. Schick, editor. Marcel Dekker, New York.
30. Carnie, S., J. N. Israelachvili, and B. A. Pailthorpe. 1979. Lipid packing and transbilayer asymmetries of mixed lipid vesicles. *Biochim. Biophys. Acta.* 554:340–357.
31. Israelachvili, J. N. 1992. Intermolecular and Surface Forces. Academic Press, London.
32. McConnell, H. M., P. A. Rice, and D. J. Benvegnu. 1990. Brownian motion of lipid domains in electrostatic traps in monolayers. *J. Phys. Chem.* 94:8965–8968.
33. Klingler, J. F., and H. M. McConnell. 1993. Field-gradient electrophoresis of lipid domains. *J. Phys. Chem.* 97:2962–2966.
34. McConnell, H. M., and A. Radhakrishnan. 2003. Condensed complexes of cholesterol and phospholipids. *Biochim. Biophys. Acta.* 1610:159–173.
35. Andelman, D., F. Brochard, and J. F. Joanny. 1987. Phase transitions in Langmuir monolayers of polar molecules. *J. Chem. Phys.* 86:3673–3681.
36. van der Schoot, P. 2005. Theory of supramolecular polymerization. *In* Supramolecular Polymers. A. Ciferri, editor. CRC Press. Boca Raton, FL. 77–106.
37. Sagui, C., and R. C. Desai. 1995. Ostwald ripening in systems with competing interactions. *Phys. Rev. Lett.* 74:1119–1122.
38. Israelachvili, J. 1973. Theoretical considerations on asymmetric distribution of charged phospholipid molecules on inner and outer layers of curved bilayer membranes. *Biochim. Biophys. Acta.* 323: 659–663.
39. Israelachvili, J. N., and D. J. Mitchell. 1975. Model for Packing of Lipids in Bilayer Membranes. *Biochim. Biophys. Acta.* 389:13–19.
40. Israelachvili, J. 1994. Self-assembly in 2 dimensions: surface micelles and domain formation in monolayers. *Langmuir.* 10:3774–3781.
41. McConnell, H. M. 1989. Theory of hexagonal and stripe phases in monolayers. *Proc. Natl. Acad. Sci. USA.* 86:3452–3455.
42. Mulder, W. H. 1997. Equilibrium size distributions of circular domains in amphiphilic monolayers. *J. Phys. Chem. B.* 101:7744–7750.
43. Wurlitzer, S., T. M. Fischer, and H. Schmiedel. 2002. Equilibrium size of circular domains in Langmuir monolayers. *J. Chem. Phys.* 116: 10877–10881.